ARTICLE TYPE www.rsc.org/xxxxxx | XXXXXXXX

Challenges in the Simulation of Dye-Sensitized ZnO: Quantum confinement, Alignment of Energy Levels and Excited States Nature at the Dye/Semiconductor Interface

Anna Amat[a] and Filippo De Angelis[b]

Received (in XXX, XXX) Xth XXXXXXXXX 200X, Accepted Xth XXXXXXXXX 200X
First published on the web Xth XXXXXXXXX 200X
DOI: 10.1039/b00000000x

We report a first principles DFT/TDDFT computational investigation on a prototypical perylene dye anchored to realistic ZnO substrates, as a model of the related DSC devices. DFT calculations were performed on different $(ZnO)_n$ clusters of increasing size, with n up to 222 of 1.3x1.3x3.0 nm dimensions, and for the related dye-sensitized models. We show that quantum confinement in the ZnO nanostructures substantially affects the dye/semiconductor alignment of energy levels, with smaller ZnO models providing unfavourable electron injection thermodynamics. An increasing mixing between dye and semiconductor unoccupied states is found moving to larger substrates, substantially contributing to the interfacial electronic coupling. TDDFT excited state calculations for the investigated dye@$(ZnO)_{222}$ system are fully consistent results with the experimental data, quantitatively reproducing the red-shift and broadening of the visible absorption spectrum observed for the ZnO-anchored dye compared to the dye in solution. TDDFT calculations on the fully interacting system also introduce a further contribution to the dye/semiconductor state admixture, due configurational excited state mixing. Our results highlight the challenges in the simulation of dye-sensitized ZnO interfaces, yet we show that a proper computational set up is able to capture the fundamental insight lying at the heart of the associated DSC devices.

Introduction

In the field of renewal energies, Dye Sensitized Solar cells (DSCs)[1-6] are a promising alternative to traditional carbon-based energy. DSCs are potentially low cost devices which can work under non-optimal and diffuse light conditions. Moreover, being coloured-transparent and flexible they have attracted great interest for architecture and design. In the last decades great effort has been devoted to the increase of the DSCs efficiencies and a growing number of papers have been published on this field.

In DSCs devices, an organic/metallorganic dye adsorbed onto the surface of a nanostructured wide band-gap semiconductor absorbs the solar radiation, thus producing a charge-transfer excited state. The resulting photoexcited electrons and holes are transferred to the semiconductor manifold of unoccupied states and to an electrolyte or hole conductor, respectively. The oxidized dye is then regenerated by the reduced species in the electrolyte. The injected electron travels through the network of semiconductor particles to reach the contact, produces an external work, and eventually reaches the cathode where the oxidized form of the electrolyte is regenerated, closing the circuit.

Even though many efforts have been focused on the generation of new dyes with improved electronic properties, the role of other components of the cell are also being actively investigated. New redox couples[7-9] have been proposed as alternatives to the standard I^-/I_3^- liquid electrolyte and alternative semiconductors, such as ZnO, SnO_2, ZrO_2, Nb_2O_5, SnO_2 and In_2O_3,[10-13] are being studied to try to rival the most widely used and efficient TiO_2-substrates. DSCs based on nanostructured TiO_2 have indeed led to the highest efficiencies to date,[14,15] with a recently achieved record of efficiency exceeding 12%[16], while for ZnO-based DSCs efficiencies up to 7.5% have been reported.[17] Despite the lower efficiency, ZnO has received considerable interest as a semiconductor substrate for DSCs due to its high electron mobility that can lead to a faster electron transport rate.[18-22] Moreover, a large variety of ZnO nanostructures have been synthesized,[23] further allowing to tuning of the electronic properties of the DSC photoanode.

Bulk ZnO and TiO_2 posses similar band gaps and conduction band edge energies,[24] but a quite different band structure, with TiO_2 showing a indirect band gap and a much larger density of states than ZnO, which shows a direct band gap. The higher density of states in TiO_2 can directly affect electron injection from the dye excited state, ensuring a strong coupling between the dye excited state and the semiconductor manifold of unoccupied states.[18,25] Interestingly, while for TiO_2 the band gap and conduction band energy edge are largely insensitive to the particle size above a minimum threshold,[25] a significant quantum confinement effect has been reported for ZnO. Band-gap variations between 3.4 and 3.8 eV have been reported for ZnO depending on the size of the nanostructures.[26-28] The band gap increase is associated to different valence and conduction band energy shifts, with the conduction band edge increasing its energy, i.e. becoming less negative vs. vacuum, when reducing the structure size.[29-30] In light of the

anticipated strong effect of the conduction band energetics, density of states and alignment with the energy levels of the excited dye on the electron injection efficiency,[25,31] significant differences between TiO_2 and ZnO can be expected when varying the dimensions of the nanostructures constituting the DSCs semiconductor film.

Computer simulations rooted into Density Functional Theory (DFT) and Time Dependent DFT (TDDFT) have become a crucial tool to understand the detailed atomistic factors ruling the DSCs efficiency. The simulation of the dye/semiconductor interface is however a formidable task, since it requires to model on the same footing the molecular dye and the extended semiconductor in the environment of the electrolyte (typically acetonitrile). As a matter of fact, the calculation of the explicitly interacting dye/semiconductor/solvent excited states has been possible only in limited cases and with a large associated computational overhead.[32]

For dye sensitized TiO_2 interfaces, we have devised over time an integrated computational protocol, based on a description of the semiconductor relying on large clusters, e.g. $(TiO_2)_{82}$,[33] which has allowed us to accurately simulate the excited state properties of the most efficient Ru(II) and organic dyes adsorbed onto TiO_2 entirely from first principles.[31,33] An alternative approach which avoids the solution of the interacting system' properties in a full quantum mechanical framework has been also reported,[34-36] in which the dye excited states are perturbed by the presence of the semiconductor in a quantum mechanics/molecular mechanics embedding fashion. This approach, however, should only hold for weakly interacting dye/semiconductor systems, which is often not the case for the most performing systems.[31,33,37]

Recently, we have set up realistic ZnO nanostructures which accurately describe the electronic and optical properties of the corresponding experimental systems.[23,38] Following this work and motivated by the high-level time-resolved spectroscopic study on the injection mechanism of perylene dyes on ZnO,[18] we aim here at extending our theoretical investigations to perylene dye-sensitized ZnO, with particular reference to the conjugated dye reported in Fig. 1. The class of perylene dyes has been extensively investigated and have shown very promising efficiency when employed in solid state devices[39] and in liquid electrolyte DSCs.[40]

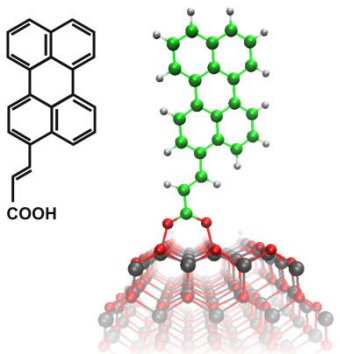

Fig. 1 Structure of the investigated perylene dye and modality of adsorption into ZnO.

We find that proper modelling of dye/ZnO interfaces turns out to be a much more challenging task than that of the corresponding TiO_2 systems, due to the pronounced ZnO quantum confinement effects which introduce substantial difficulties in reproducing the dye/semiconductor mixing and alignment of energy levels. We thus investigate saturated $(ZnO)_n$ clusters of increasing dimensions, up to n=222 of ca. 1.3x1.3x3.0 nm dimensions, which show a progressively lower conduction band energy edge, finding that the mixing of dye/semiconductor molecular orbitals and the nature of the excited states substantially changes with the semiconductor size and eventually strongly affects the electronic coupling across the dye-sensitized semiconductor interface. Our results highlight the very relevant role and the challenge of properly describing the nature and the alignment of excited state energy levels at the dye/ZnO interface, opening the way to the accurate simulation of dye-sensitized ZnO solar cells.

Model and computational details

To model ZnO nanostructures of increasing dimensions $(ZnO)_{42}$, $(ZnO)_{84}$ and $(ZnO)_{222}$ clusters have been built, see the optimized geometries in Fig 1. To avoid the metallization of the semiconductor due to the polar Zn- and the O-terminated surfaces, proper saturation has been applied with dissociated water molecules, as reported in our previous work.[23]

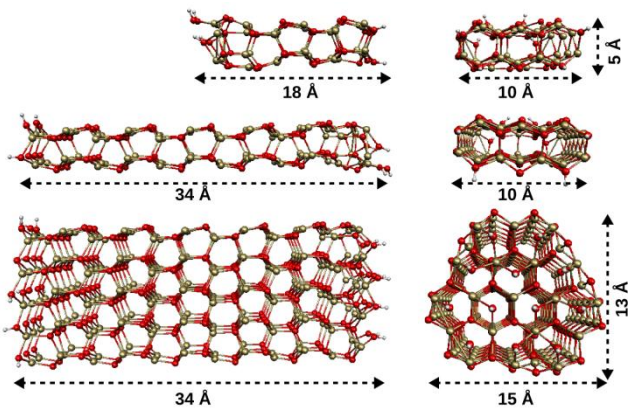

Fig.1 Optimized geometrical structures of the investigated $(ZnO)_{42}$, $(ZnO)_{84}$ and $(ZnO)_{222}$ clusters.

The semiconductor and dye@semiconductor models have been optimized in vacuo using the BPW91 exchange-correlation functional,[41] as implemented in the ADF program package.[42] For simplicity, we considered the dye to adsorb in its deprotonated state in a bridged bidentate configuration on the apolar (1010) surface, see Figure 2. Subsequent DFT and TDDFT calculations have been performed on the optimized structures using the B3LYP exchange-correlation functional,[43-45] a 6-31G* basis set[46,47] and including solvation effects by means of the conductor-like polarizable continuum model of solvation (CPCM),[48-51] as implemented in Gaussian03.[52] The absorption spectra have been simulated by using a convolution of Gaussian functions with an FWHM = 0.25 eV.

Results and Discussion

The focus of this work is on the electronic structure and optical properties of the perylene derivative with a conjugated acrylic acid anchoring group, Fig. 1, hereafter simply the dye, adsorbed onto ZnO. This system has been investigated by

time-resolved spectroscopic techniques,[18] finding quite a strong dye/semiconductor coupling, as signalled by the broader and partly unstructured steady-state absorption spectrum measured for the dye anchored to the semiconductor compared to the dye in solution. Coherently with this observation, a 190 fs fast electron injection component was measured for the dye@ZnO. Stronger coupling and shorter injection times were found for TiO_2 compared to ZnO.[18] Considering the charge injection as a non-adiabatic radiationless process, the dye/semiconductor coupling can be directly related to the electron injection rate constant by using the Fermi's golden rule.[25] In this framework, the injection rate depends on two factors: i) the density of available states of the semiconductor, and ii) the electronic coupling between the donor and the acceptor.[25] The first (second) term is related to the alignment (mixing) of dye/semiconductor energy levels, which therefore both contribute to the electron injection process.

Electronic structure

We start by investigating the electronic structure of three $(ZnO)_n$ models of increasing size, with n=42, 84 and 222, and of the corresponding dye@$(ZnO)_n$ systems. The results for the non interacting and interacting dye@$(ZnO)_n$ structures (for n=42 and 222) are reported in Fig. 3.

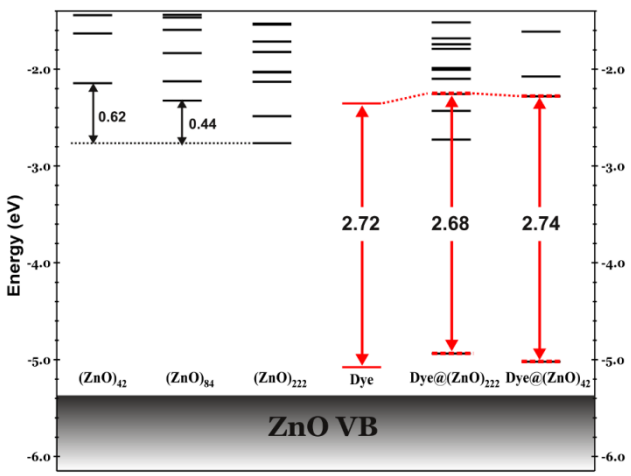

Fig. 2 Schematic energy levels of the isolated Dye and $(ZnO)_n$ clusters (n=42, 84 and 222) and of the interacting Dye@$(ZnO)_n$ (n=42 and 222) systems. Levels which are maximally localized on the dye are in red.

Comparing the isolated $(ZnO)_n$ systems, we immediately notice that the ZnO conduction band edge, corresponding to the systems' LUMO, substantially down-shifts on going from n=42 to 84 and to 222 ZnO units, with 0.18 and 0.62 eV shifts, respectively. For the non-interacting dye and n=42 and 84 systems, the lowest semiconductor unoccupied state lies above or is almost coincident with the dye-based LUMO, making electron injection energetically unfavourable. For the large $(ZnO)_{222}$ cluster, on the other hand, the ZnO-based LUMO lies ca. 0.4 eV below the dye-based LUMO, reverting the dye/semicondutor energetics and making electron injection a favoured process. Concerning the band gap of the investigated $(ZnO)_n$ models, we find values of 3.43, 3.04 and 2.67 eV for n=42, 84, 222 respectively. These results are underestimated compared to expected band gaps for small nanostructures, e.g. ca. 3.5-3.6 eV,[26,27] but since we are interested here in the conduction band energetics the HOMO-LUMO gap underestimate, mainly due to the valence band energy upshift,[23] is believed not to affect the subsequent results.

For the interacting dye/ZnO system we find a similar alignment of energy levels as for the non-interacting systems, Fig. 3; the energy and the composition of the frontier molecular orbitals of the Dye@$(ZnO)_n$ systems in terms of dye and semiconductor contributions are reported in Table 1.

Table 1 Highest occupied and lowest unoccupied molecular orbital energies (eV) and compositions for the Dye@$(ZnO)_n$, with n=42 and 222.

	Dye@$(ZnO)_{42}$			Dye@$(ZnO)_{222}$		
State	**Energy**	**Dye**	**ZnO**	**Energy**	**Dye**	**ZnO**
HOMO	-5.03	99%	1%	-4.94	91%	9%
LUMO	-2.28	95%	5%	-2.73	0%	100%
LUMO+1	-2.07	1%	99%	-2.43	0%	100%
LUMO+2	-1.61	1%	99%	-2.26	87%	13%
LUMO+3	-1.39	0%	100%	-2.10	0%	100%

For both Dye@$(ZnO)_{42}$ and Dye@$(ZnO)_{222}$ we calculate the almost pure dye HOMO to insert within the semiconductor band-gap; this level is only marginally affected by the size of the ZnO cluster. On the contrary, as found for the non-interacting systems, the position of the semiconductor-based LUMO is strongly dependent on the system size. For Dye@$(ZnO)_{42}$, the LUMO is mainly localized on the dye, with the lowest unoccupied level localized on the ZnO lying 0.11 eV above. For Dye@$(ZnO)_{222}$, on the other hand, the LUMO is manly located on the semiconductor, with the first unoccupied orbital localized on the dye being the LUMO+2, found 0.47 eV above the LUMO. Furthermore, while the dye-based LUMO has only a 5% mixing with ZnO states for Dye@$(ZnO)_{42}$, for Dye@$(ZnO)_{222}$ a 13% contribution to the dye-based LUMO+2 comes from the semiconductor. These differences can be clearly visualized in the isodensity plots reported for the relevant orbitals in Fig. 4. In a previous investigation of the same dye on TiO_2,[53] we found the interacting dye/semiconductor LUMO to be distributed by 15% and 85% in the dye and the semiconductor, respectively. This reflects, in comparison with the ZnO substrate, the much stronger electronic coupling and the shorter injection times experimentally observed for TiO_2 compared to ZnO.[18]

To summarize this section, we have shown how the size of the ZnO substrate affects the band alignment energetics and consequently the mixing between dye and semiconductor molecular orbitals, which are the two fundamental parameters affecting the electron injection from the dye excited state into the manifold of unoccupied semiconductor states.[25]

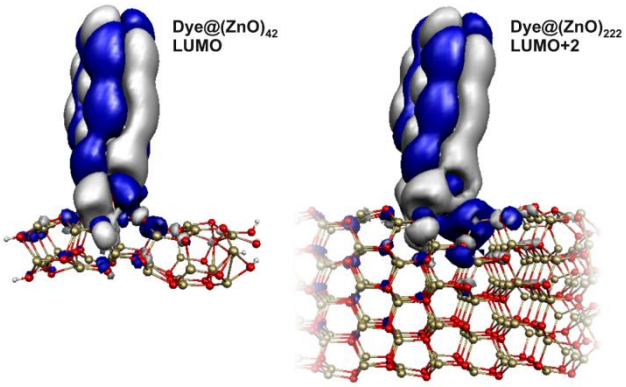

Fig. 4 Isodensity plots (0.001 isodensity) of the LUMO and LUMO+2 states for Dye@$(ZnO)_{42}$ and Dye@$(ZnO)_{222}$ systems. Notice the larger ZnO contribution to the dye-based LUMO+2 in Dye@$(ZnO)_{222}$. For clarity, only the dye-anchoring region is shown for the Dye@$(ZnO)_{222}$ system.

Excited states

To gain further insight on the Dye@$(ZnO)_n$ excited state nature beyond a simple one-electron picture, we performed TDDFT excited state calculations for both the n=42 and n=222 cases. For the latter system, TDDFT calculations were particularly heavy, involving 4362 occupied orbitals and 11951 basis functions, so we were able to calculate only the lowest seven excited states in the fully interacting orbital space. The computed absorption spectra for the Dye@$(ZnO)_n$ systems (n=42 and 222) are compared to results for the isolated dye in solution and to experimental data in Figure 5, while a list of the main computed transitions along with their character in terms of constituting molecular orbitals are reported in Table 2.

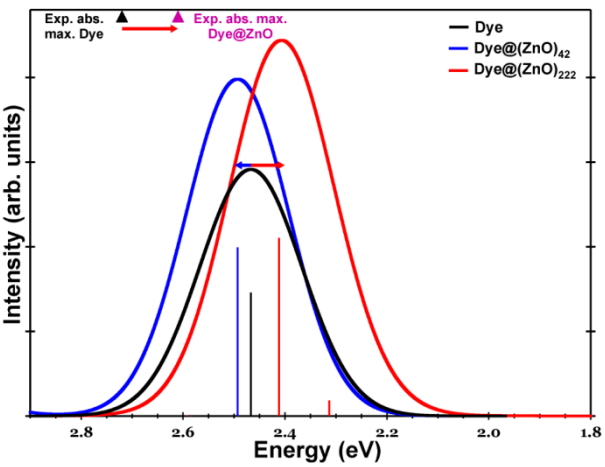

Fig. **5** TDDFT-calculated absorption spectra for the isolated dye (black line) and for the Dye@$(ZnO)_{42}$ (blue line) and the Dye@$(ZnO)_{222}$ (red-line) systems. Vertical lines correspond to unbroadened excitation energies and oscillator strengths. The experimental absorption maxima values for the isolated dye and for the dye-sensitized ZnO from ref. 18 are also reported with black and magenta markers, respectively.

Table 2 Computed TDDFT excited states for the Dye@$(ZnO)_{42}$ and Dye@$(ZnO)_{222}$ systems. The energy (eV), oscillator strength and decomposition in terms of molecular orbitals reported.

	Dye@$(ZnO)_{42}$			**Dye@$(ZnO)_{222}$**		
Exc. state	**Energy**	**f**	**Composition**	**Energy**	**f**	**Composition**
S_1	2.49	1.00	80% H->L	2.04	0.00	99% H->L
S_2	2.72	0.00	100% H->L+1	2.31	0.09	54% H-1->L 34% H->L+1 6% H-1->L+1 2% H->L+2
S_3	3.02	0.01	83% H-1->L+1 8% H-1->L+2	2.34	0.00	63% H->L+1 35% H-1->L
S_4	3.05	0.00	93% H-1->L 6% H-1->L+1	2.41	1.05	76% H->L+2 3% H-1->L 2% H-1->L+2

Experimentally, an absorption maximum at 2.72 eV is measured for the isolated dye in methanol solution, while dye anchoring onto the ZnO surface produces an absorption maximum red-shift of ca. 0.10 eV.[18] The computed absorption spectrum of the isolated dye is formed by a single HOMO→LUMO excitation computed at 2.47 eV, i.e. 0.25 eV red-shifted compared to the experimental data.[53] The absorption spectrum of the Dye@$(ZnO)_{42}$ system is dominated by a single transition ($S_0 \rightarrow S_1$) computed at 2.49 eV, of essentially (80%) HOMO→LUMO character. Recalling the nature of the involved orbitals from Table 1, this implies essentially a charge-redistribution taking place within the dye, with negligible coupling to semiconductor unoccupied states. Furthermore, the absorption maximum is slightly blue-shifted with respect to the isolated dye, contrary to the experimental findings.

For the Dye@$(ZnO)_{222}$ system, we calculate the absorption maximum at 2.41 eV, i.e. 0.06 eV red-shifted compared to the isolated dye molecule in solution, as experimentally retrieved. The spectrum is mainly formed by two transitions: i) $S_0 \rightarrow S_2$, computed at 2.31 eV, characterized by a small but sizable oscillator strength (0.09), and ii) the more intense $S_0 \rightarrow S_4$ excitation, computed at 2.41 eV, with an oscillator strength of 1.05. The lowest excitation, $S_0 \rightarrow S_1$, is calculated at 2.04 eV with zero oscillator strength, see Table 1, and corresponds to a direct charge-transfer excitation from the dye-based HOMO to the ZnO-based LUMO. The $S_0 \rightarrow S_2$ excitation is made of contributions from four major orbital excitations; these are mainly localized within the semiconductor, although they are characterized by a small admixture with dye states. The intense $S_0 \rightarrow S_4$ excitation is mainly formed by a HOMO → LUMO+2 transition, with the latter orbital showing 87% and 13% localization within the dye and semiconductor, respectively.

The differences between the n=42 and n=222 cases clearly point out how the mixing of the dye excited state and the unoccupied orbitals of the ZnO substrate is highly dependent on the semiconductor size. For the $(ZnO)_{222}$ cluster, the lowering of the unoccupied semiconductor energy levels introduces a sizable mixing between these states and the lowest unoccupied orbital localized on the dye. Such mixing leads to a new optical transition in the absorption spectrum with large semiconductor character and it also contributes substantial semiconductor character to the main optical transition, definitely increasing the coupling between dye and semiconductor excited states, thus facilitating electron injection. On the contrary, for the smaller $(ZnO)_{42}$ cluster, the

unoccupied semiconductor orbitals lay above the lowest unoccupied state localized on the dye, impeding any sizable coupling. Indeed, for Dye@$(ZnO)_{42}$ the absorption spectrum shows a single excitation to an unoccupied state having only a 5% contribution from the semiconductor.

A more complete vision of the overall character and localization of excited state at the dye/semiconductor interface for n=42 and 222 can be obtained by plotting the absolute values of the charge differences between the excited states involved in the main excitations and the ground state, $|\Delta\rho|=|\rho(S_n) - \rho(S_0)|$. This quantity allows for the visualization of the excited state localization, whereby the absolute value serves to exclude possible $\Delta\rho$ cancellations due to sign changes within a given region of space which would show up upon $\Delta\rho$ integration. We have computed $|\Delta\rho|$ curves for the S_0-S_1 and S_0-S_4 transitions of Dye@$(ZnO)_{42}$ and Dye@$(ZnO)_{222}$, respectively, the results are reported in Fig. 6. For each system, we define the z coordinate as the dye axis normal to the semiconductor surface and integrate the charge differences along the x and y directions.

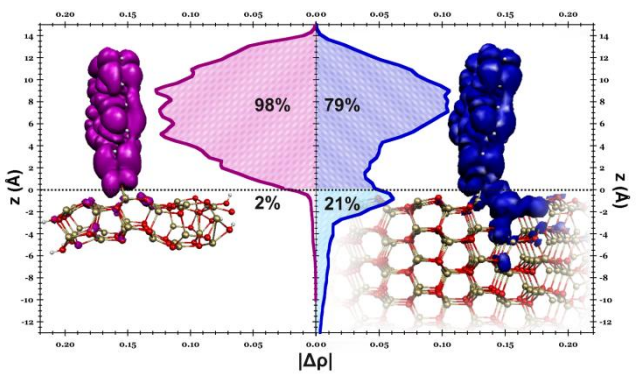

Fig. 6 Isodensity plot of the absolute charge difference differences ($|\Delta\rho|$) between S_0-S_1 of Dye@$(ZnO)_{42}$ (left, magenta) and S_0-S_4, of Dye@$(ZnO)_{222}$ (right, blue). Center: Integral of $|\Delta\rho|$ along the x and y directions plotted as a function of z. The zero is in all cases set in the middle of the O-Zn bonds between the dye and the semiconductor.

As it can be observed from Figure 6, for both n=42 and n=222 the most intense excitations are primarily located in the dye space region. Noticeable differences are however found at the dye/semiconductor interface for the two systems. The Dye@$(ZnO)_{42}$ system exhibits a negligible excited state spreading into the semiconductor, as it can be quantitatively seen from the isodensity $|\Delta\rho|$ plot and from the integrated $|\Delta\rho|$ curve. On the contrary, for Dye@$(ZnO)_{222}$ the isodensity $|\Delta\rho|$ plot clearly shows a sizable contribution from the semiconductor, being characterized by a 79/21% dye/semiconductor localization. It is worth to notice that this value, obtained from excited states calculations, is larger than the 87/13% dye/semiconductor localization retrieved from the one-electron molecular orbital analysis of Table 1, due to the additional configurational mixing between dye and semiconductor states introduced by the TDDFT calculation.

Our results clearly show that a substantial coupling between the dye and the large ZnO model exists. This is due both to orbital and excited state configuration mixing, both imparting a substantial semiconductor character to the otherwise dye optical transitions. The sizable dye/semiconductor mixing and the calculated alignment of energy levels are perfectly in line with the measured ultrafast electron injection dynamics.

Concluding Remarks

We have reported a first principles DFT/TDDFT computational investigation on a prototypical perylene dye anchored to realistic ZnO substrates, as a model of the related DSCs devices.

DFT calculations were performed on three different $(ZnO)_n$ clusters of increasing size, with n=42, 84 and 222, up to realistic 1.3x1.3x3.0 nm ZnO substrate dimensions and for the related dye-sensitized models. We have shown that quantum confinement in the ZnO nanostructures substantially affects the dye/semiconductor alignment of energy levels, with smaller ZnO models providing unfavourable electron injection pathways. Along with the shifts of the energy levels, a substantial mixing between dye and semiconductor unoccupied states is found when moving to the largest investigated system, substantially contributing to the interfacial electronic coupling. To move beyond a single orbital picture, we carried out TDDFT excited state calculations for the dye@$(ZnO)_{222}$ system, providing fully consistent results with the corresponding experimental data. In particular, for such a complex system, we are able to quantitatively reproduce the red-shift and broadening of the visible absorption spectrum in going from the dye in solution to the dye anchored to the ZnO surface, which signals a substantial electronic coupling. TDDFT calculations on the fully interacting system are also found to introduce a further contribution to the dye/semiconductor state admixture, due configurational excited state mixing. The sizable dye/semiconductor coupling and the calculated alignment of energy levels, showing ca. 0.4 eV driving force for electron injection, are perfectly in line with the measured ultrafast injection dynamics for this system.

Our results highlight the challenges in the simulation of dye-sensitized ZnO interfaces, yet we show that a proper computational set up based on extended semiconductor models and extensive TDDFT excited state calculations is able to capture the fundamental insight lying at the heart of the associated DSCs devices.

Acknowledgments

We thank FP7-ENERGY 2010 261920-ESCORT and FP7-NMP-2009 246124-SANS for financial support. FDA thanks Fondazione Istituto Italiano di Tecnologia, Platform Computation, Project SEED 2009 “HELYOS” for a grant.

Notes and references

[a] *Istituto CNR di Scienze e Tecnologie Molecolari (ISTM), c/o Dipartimento di Chimica, Università di Perugia, Via elce di Sotto 8, I-06213, Perugia, Italy.*

* *E-mail: filippo@thch.unipg.it*

1 B. O'Regan and M. Grätzel, *Nature*, 1991**, 353**, 737-740.
2 J. M. Rehm, G. L. McLendon, Y. Nagasawa, K. Yoshihara, J. Moser, and M. Grätzel, *J. Phys. Chem. B*, 1996, **100**, 9577-9578.
3 A. Hagfeldt and M. Grätzel, *Chem. Rev.*, 1995, **95**, 49-68.
4 M. Grätzel, *Nature*, 2001, **414**, 338-344.
5 M. K. Nazeeruddin, Q. Wang, L. Cevey, V. Aranyos, P. Liska, E. Figgemeier, C. Klein, N. Hirata, S. Koops, S. A. Haque, J. R. Durrant, A. Hagfeldt, A. B. P. Lever and M. Grätzel, *Inorg. Chem.*, 2006, **45**, 787-797.
6 P. V. Kamat, *J. Phys. Chem. C*, 2007, **111**, 2834-2860.
7 Y. Liu, J. R. Jennings, Y. Huang, Q. Wang, S. M. Zakeeruddin and M. Grätzel, *J. Phys. Chem. C*, 2011, **115**, 18847-18855.
8 S. M. Feldt, E. A. Gibson, E. Gabrielsson, L. Sun, G. Boschloo and A. Hagfeldt, *J. Am. Chem. Soc.*, 2010, **132**, 16714-16724.
9 M. Wang, N. Chamberland; L. Breau, J-E. Moser, R. Humphry-Baker, B. Marsan, S. M. Zakeeruddin and M. Grätzel, *Nature Chemistry*, 2010, **2**, 385-389.
10 R. Katoh, A. Furube, T. Yoshihara, K. Hara, G. Fujihashi, S. Takano, S. Murata, H. Arakawa and M. Tachiya, *J. Phys. Chem. B*, 2004, **108**, 4818-4822.
11 T. Yoshida, J. Zhang, D. Komatsu, S. Sawatani, H. Minoura, T. Pauporté, D. Lincot, T. Oekermann, D. Schlettwein, H. Tada, D. Wöhrle, K. Funabiki, M. Matsui, H. Miura and H. Yanagi, *Adv. Funct. Mat.*, 2009, **19**, 17-43.
12 O. Lupan, V. M. Guérin, I. M. Tiginyanu, V. V. Ursaki, L. Chow, H. Heinrich and T. Pauporté, *J. of Photochem. and Photobiol. A: Chemistry*, 2010, **211**, 65-73.
13 F. Odobel, L. Le Pleux, Y. Pellegrin and E. Blart, *Acc. Chem. Res.*, 2010, **43**, 1063-1071.
14 M. K. Nazeeruddin, F. De Angelis, S. Fantacci, A. Selloni, G. Viscardi, P. Liska, S. Ito, T. Bessho and M. Gratzel, *J. Am. Chem. Soc.*, 2005, **127**, 16835-16847.
15 Y. Chiba, A. Islam, Y. Watanabe, R. Komiya, N. Koide and L. Han, *Japanese J. of App. Phys*, 2006, **45**, L638-L640.
16 A. Yella, H-W. Lee, H. N. Tsao, C. Yi, A. K. Chandiran, M. K. Nazeeruddin, E. W. Diau, C-Y. Yeh, S. M. Zakeeruddin and M. Grätzel, *Science*, 2011, **334**, 629-634.
17 N. Memarian, I. Concina, A. Braga, S. M. Rozati, A. Vomiero and G. Sberveglieri, *Angew. Chem.*, 2011, **123**, 12529 -12533.
18 J. M. Szarko, A. Neubauer, A. Bartelt, L. Socaciu-Siebert, F. Birkner, K. Schwarzburg, T. Hannappel and R. Eichberger, *J. Phys. Chem. C*, 2008, **112**, 10542-10552.
19 E. Galoppini, J. Rochford, H. Chen, G. Saraf, Y. Lu, A. Hagfeldt and G. Boschloo, *J. Phys. Chem. B*, 2006, **110**, 16159-16161.
20 J. Baxter and E. Aydil, *Appl. Phys. Lett.*, 2005, **86**, 053114-053116.
21 M. Law, L. Greene, J. Johnson, R. Saykally and P. Yang, *Nat. Mater.*, 2005, **4**, 455-459.
22 M. Boucharef, C. Di Bin, M. S. Boumaza, M. Colas, H. J. Snaith, B. Ratier and J. Boucle, *Nanotech.*, 2010, **21**, 205203-205214.
23 F. De Angelis and L. Armelao, *Phys. Chem. Chem. Phys*., 2011, **13**, 467-475.
24 B. O'Regan, V. Sklover and M. Gratzel, *J. of the Electrochem. Soc.*, 2001, **148**, C498-C505.
25 J. E. Moser, In *Dye-Sensitized solar cells;* K. Kalyanasundaram, Ed. EPFL Press, Lausanne, 2010**; Vol. 11.** pp 403-456.
26 S. Monticone, R. Tufeu and A. V. Kanaev, *J. Phys. Chem. B*, 1998, **102**, 2854-2862.
27 A. van Dijken, E. A. Meulenkamp, D. Vanmaekelbergh and A. Meijerink, *J. Phys. Chem. B*, 2000, **104**, 1715-1723.
28 M. L. Kahn, T. Cardinal, B. Bousquet, M. Monge, V. Jubera and B. Chaudret, *ChemPhysChem*, 2006, **7**, 2392-2397.
29 R. Viswanatha, S. Sapra, B. Satpati, P. V. Satyam, B. N. Dev and D. D. Sarma, *J. Mater. Chem.*, 2004, **14**, 661-668.
30 T. G. Pedersen, *Phys. Stat. Sol. (c)*, 2005, **2**, 4026-4030.
31 F. De Angelis, S. Fantacci, E. Mosconi, M. K. Nazeeruddin and M. Graetzel, *J. Phys. Chem. C*, **2011**, 115, 8825-8831.
32 F. De Angelis, S. Fantacci and R. Gebauer, *J. Phys. Chem. Lett.*, 2011, **2**, 813-817.
33 F. De Angelis, S. Fantacci, A. Selloni, M. K. Nazeeruddin and M. Grätzel, *J. Phys. Chem. C*, 2010, **114**, 6054-6061.
34 F. Labat, I. Ciofini, H. P. Hratchian, M. J. Frisch, K. Raghavachari and C. Adamo, *J. Am. Chem. Soc.*, 2009, **131**, 14290-14298.
35 T. Le Bahers, F. Labat, T. Pauporté, P. P. Lainé and I. Ciofini, *J. Am. Chem. Soc.*, 2011, **133**, 8005-8013.
36 F. Labat, I. Ciofini, H. P. Hratchian, M. J. Frisch, K. Raghavachari and C. Adamo, *J. Phys. Chem. C*, 2011, **115**, 4297-4306.
37 F. De Angelis, S. Fantacci, A. Selloni, M. K. Nazeeruddin and M. Grätzel, *J. Am. Chem. Soc.*, 2007, **129**, 14156-14157.
38 J. M. Azpiroz, E. Mosconi and F. De Angelis, *J. Phys. Chem. C*, 2011, **115**, 25219-25226.
39 U. B. Cappel, M. H. Karlsson, N. G. Pschirer, F. Eickemeyer, J. Schöneboom, P. Erk, G. Boschloo and A. Hagfeldt, *J. Phys. Chem. C*, 2009, **113**, 14595-14597.
40 C. Li, J-H. Yum, S-J. Moon, A. Herrmann, A.; F. Eickemeyer, N.G. Pschirer, P. Erk, J. Schöneboom, K. Müllen, M. Grätzel and M. K. Nazeeruddin, *ChemSusChem*, 2008, **1**, 615-618.
41 a) A. D. Becke, *Phys. Rev. A*, 1988, **38**, 3098100; b) J. P.;Perdew, J. A. Chevary, S. H. Vosko, K. A. Jackson, M. R. Pederson, D. J. Singh and C. Fiolhais, *Phys. Rev. B*, 1992, **46**, 667187.
42 G. Velde, F. M. Bickelhaupt, E. J. Baerends, C. Fonseca Guerra, S. J. A. van Gisbergen, J. G. Snijders and T. Ziegler, *J. Comput. Chem.*, 2001, **22**, 931-967.
43 A. D. Becke, *J. Chem. Phys.*, 1998, 98**,** 5648-5652.
44 C. Lee, W. Yang and R. G. Parr, *Phys. Rev. B*, 1988, **37**, 785-789.
45 B. Miehlich, A. Savin, H. Stoll and H. Preuss, *Chem. Phys. Lett.*, 1989, **157**, 200-206.
46 G. A. Petersson, A. Bennett, T. G. Tensfeldt, M. A. Al-Laham, W. A. Shirley and J. Mantzaris, *J. Chem. Phys.*, 1998, **89**, 2193-2218.
47 G. .A Petersson and M. A. Al-Laham, *J. Chem. Phys.*, 1991, **94**, 6081-6090.
48 V. Barone and M. Cossi, *J. Phys. Chem. A*, 1998, **102**, 1995-2001.
49 M. Cossi, N. Rega, G. Scalmani and V. Barone, *J. Comput. Chem.*, 2003, **24**, 669-681.
50 M. Cossi and V. Barone, *J. Phys. Chem. A*, 2000, **104**, 10614-10622.
51 M. Cossi, M and V. Barone, V. *J. Chem. Phys.* 2001, **115**, 4708-4717.
52 Gaussian 03, Revision C.02, M. J. Frisch, G. W. Trucks, H. B. Schlegel, G. E. Scuseria, M. A. Robb, J. R. Cheeseman, J. A. Montgomery, Jr., T. Vreven, K. N. Kudin, J. C. Burant, J. M. Millam, S. S. Iyengar, J. Tomasi, V. Barone, B. Mennucci, M. Cossi, G. Scalmani, N. Rega, G. A. Petersson, H. Nakatsuji, M. Hada, M. Ehara, K. Toyota, R. Fukuda, J. Hasegawa, M. Ishida, T. Nakajima, Y. Honda, O. Kitao, H. Nakai, M. Klene, X. Li, J. E. Knox, H. P. Hratchian, J. B. Cross, V. Bakken, C. Adamo, J. Jaramillo, R. Gomperts, R. E. Stratmann, O. Yazyev, A. J. Austin, R. Cammi, C. Pomelli, J. W. Ochterski, P. Y. Ayala, K. Morokuma, G. A. Voth, P. Salvador, J. J. Dannenberg, V. G. Zakrzewski, S. Dapprich, A. D. Daniels, M. C. Strain, O. Farkas, D. K. Malick, A. D. Rabuck, K. Raghavachari, J. B. Foresman, J. V. Ortiz, Q. Cui, A. G. Baboul, S. Clifford, J. Cioslowski, B. B. Stefanov, G. Liu, A. Liashenko, P. Piskorz, I. Komaromi, R. L. Martin, D. J. Fox, T. Keith, M. A. Al-Laham, C. Y. Peng, A. Nanayakkara, M. Challacombe, P. M. W. Gill, B. Johnson, W. Chen, M. W. Wong, C. Gonzalez, and J. A. Pople, Gaussian, Inc., Wallingford CT, 2004.
53 F. De Angelis, *Chem. Phys. Lett.*, 2010, **493**, 323–327.